Title: *Scn1a*-GFP transgenic mouse revealed Nav1.1 expression in neocortical pyramidal tract projection neurons

Authors: Tetsushi Yamagata[1, 2, ¶], Ikuo Ogiwara[2, 3, ¶], Tetsuya Tatsukawa[2, ¶], Yuka Otsuka[1], Emi Mazaki[2, †], Ikuyo Inoue[2, ‡], Natsuko Tokonami[2, §], Yurina Hibi[1], Shigeyoshi Itohara[4], and Kazuhiro Yamakawa[1, 2, *]

Affiliations:

[1]Department of Neurodevelopmental Disorder Genetics, Institute of Brain Science, Nagoya City University Graduate School of Medical Sciences, Nagoya, Aichi 467-8601, Japan.

[2]Laboratory for Neurogenetics, RIKEN Center for Brain Science, Wako, Saitama 351-0198, Japan.

[3]Department of Physiology, Nippon Medical School, Tokyo 113-8602, Japan.

[4]Laboratory for Behavioral Genetics, RIKEN Center for Brain Science, Wako, Saitama 351-0198, Japan.

[¶]These authors contributed equally to this work.

[†]Present address; International Research Center for Neurointelligence (IRCN), The University of Tokyo, Institutes for Advanced Study, Tokyo 113-0033, Japan.

[‡]Present address; Medical-risk Avoidance based on iPS Cells Team, RIKEN Center for Advanced Intelligence Project, Kyoto 606-8507, Japan.

[§]Present address; Institute of Physiology, University of Zürich, CH-8057 Zürich, Switzerland.

[*]Correspondence and requests for materials should be addressed to K.Y. (E-mail: yamakawa@med.nagoya-cu.ac.jp)

Abstract

Expressions of voltage-gated sodium channels Nav1.1 and Nav1.2, encoded by *SCN1A* and *SCN2A* genes, respectively, have been reported to be mutually exclusive in most brain regions. In adult neocortex, Nav1.1 is dominant in inhibitory neurons while Nav1.2 is dominant in excitatory neurons. Although a distinct subpopulation of neocortical excitatory neurons was also reported to express Nav1.1, their nature has been uncharacterized. By using newly-generated transgenic mouse lines expressing *Scn1a* promoter-driven green fluorescent protein (GFP), here we confirm mutually-exclusive expressions of Nav1.1 and Nav1.2, absence of Nav1.1 in hippocampal excitatory neurons, and further show that among neocortical excitatory neurons Nav1.1 is expressed in pyramidal tract and a subpopulation of cortico-cortical while Nav1.2 in cortico-striatal, cortico-thalamic and a distinct subpopulation of cortico-cortical projection neurons. These observations now contribute to the elucidation of pathological neural circuits for epilepsies and neurodevelopmental disorders caused by *SCN1A* and *SCN2A* mutations including sudden death in Dravet syndrome.

Introduction

Voltage-gated sodium channels (VGSCs) play crucial roles in the generation and propagation of action potentials, contributing to excitability and information processing (Catterall, 2012). They consist of one main pore-forming alpha- and one or two subsidiary beta-subunits that regulate kinetics or subcellular trafficking of the alphas. Human has nine alphas (Nav1.1~Nav1.9) and four betas (beta-1~beta-4). Among alphas, Nav1.1, Nav1.2, Nav1.3 and Nav1.6, encoded by *SCN1A*, *SCN2A*, *SCN3A* and *SCN8A*, respectively, are expressed in central nervous system. Although all these four genes show mutations in a wide spectrum of neurological diseases such as epilepsy, autism spectrum disorder and intellectual disability, two of those, *SCN1A* and *SCN2A,* are major ones (reviewed in Yamakawa et al., 2016; Meisler et al., 2021).

We previously reported that expressions of Nav1.1 and Nav1.2 are mutually-exclusive in many brain regions (Yamagata et al., 2017). In adult neocortex and hippocampus, Nav1.1 is dominantly expressed in medial ganglionic eminence (MGE)-derived parvalbumin-positive (PV-IN) and somatostatin-positive (SST-IN) inhibitory neurons (Ogiwara et al., 2007; Lorincz and Nusser, 2008; Ogiwara et al., 2013; Li et al., 2014; Tai et al., 2014; Tian et al., 2014; Yamagata et al, 2017), and some amount is also expressed in a distinct subset of neocortical layer V (L5) excitatory neurons (Ogiwara et al., 2013), the nature is unknown, but not in hippocampal excitatory neurons (Ogiwara et al., 2007; Ogiwara et al., 2013; Yamagata et al., 2017). In contrast, a major amount of Nav1.2 (~95%) is expressed in excitatory neurons including the major population of neocortical and all of hippocampal ones, and a minor amount is expressed in caudal ganglionic eminence (CGE)-derived inhibitory neurons such as vasoactive intestinal polypeptide (VIP)-positive ones (VIP-IN) (Lorincz and Nusser 2010; Yamagata et al., 2017; Ogiwara et al., 2018), however a recent study reported that a subpopulation (mostly half) of VIP-IN are Nav1.1-positive (Goff and Goldberg, 2019).

VGSCs are dominantly localized at axons and therefore it is not always easy to identify their origins, soma. To overcome this, here in this study we generated bacterial artificial chromosome (BAC) transgenic mouse lines that express GFP under the control of *Scn1a* promoters, and we carefully investigated the Nav1.1 distribution in mouse brain. Our analysis confirmed the mutually-exclusive expressions of Nav1.1 and Nav1.2, the absence of Nav1.1 in hippocampal excitatory neurons, and by using neocortical projection neuron markers FEZF2 and TBR1, newly revealed that among neocortical excitatory neurons Nav1.1 is expressed in L5 pyramidal tract and a subpopulation of L2/3 cortico-cortical neurons while Nav1.2 is expressed in L5/6 cortico-striatal, L6 cortico-thalamic and a distinct subpopulation of L2/3

cortico-cortical projection neurons.

Results

GFP signals in *Scn1a*-GFP transgenic mice faithfully reflect Nav1.1 expression

Scn1a-GFP founder mice were generated from the C57BL/6J zygotes microinjected with a modified *Scn1a*-GFP BAC construct harboring all, upstream and downstream, *Scn1a*-promoters (Nakayama et al., 2010) (Figure 1A) (See Materials and Methods for details). Western blot analysis and immunohistochemistry showed robust GFP expression and normal Nav1.1 expression in the *Scn1a*-GFP lines descending from #233 and #184 lines (Figure 1B, C). Fluorescence imaging showed relatively intense GFP signals in the caudal brain portions (Figure 1D), which is well consistent with the previously reported regional distribution of Nav1.1 protein and *Scn1a* mRNA in wild-type mouse brain (Ogiwara et al, 2007). Immunohistochemical double-staining of Nav1.1 and GFP revealed Nav1.1-signals at axon initial segments (AISs) of most neocortical and hippocampal GFP-positive cells (Figure 1E, F). In addition, double *in situ* hybridization of *Scn1a* and GFP mRNAs showed that *Scn1a* signals well overlap with neocortical and hippocampal GFP-positive cells (Figure 1G-J).

The *Scn1a*-GFP lines #184 and 233 showed a similar distribution of GFP-signals, immunoreactive and fluorescent signals as well, across the entire brain (Figure 1C, 2A-L). In neocortex (Figure 2B, F, J), GFP-positive cells were sparsely distributed throughout all cortical layers. In hippocampus (Figure 2C, G, K), GFP-immunoreactive signals, which are assumed to be PV-IN and SST-IN (Ogiwara et al, 2007; Tai et al., 2014; Yamagata 2017), were scattered in stratum oriens, pyramidale, radiatum, lucidum and lacunosum-moleculare of the CA (Cornet d'Ammon) fields and hilus and molecular layer of dentate gyrus. Note that GFP immunoreactive signals clinging around CA pyramidal but not dentate granule cells (Figure 2C, G) are axon terminals of PV-INs (Ogiwara et al., 2013), and GFP fluorescent signals are well negative in CA pyramidal and dentate granule cells (Figure 2K), confirming that these hippocampal excitatory neurons themselves are all negative for Nav1.1. In cerebellum (Figure 2D, H, L), GFP signals appeared in Purkinje, basket, and deep cerebellar nuclei cells.

All of these GFP distributions in *Scn1a*-GFP transgenic mice are well consistent to the previous reports of regional distribution of Nav1.1 protein and *Scn1a* mRNA in wild-type mouse brain (Ogiwara et al, 2007; Ogiwara 2013; Yamagata 2017). These data indicate that GFP signals in the *Scn1a*-GFP lines faithfully reflect endogenous *Scn1a*/Nav1.1 expression. In the following analyses, we used the line #233 which show stronger GFP signals than #184.

GFP signals of *Scn1a*-GFP mice do not overlap with Nav1.2

We previously reported that expressions of Nav1.1 and Nav1.2 are mutually-exclusive in many brain regions (Yamagata et al., 2017). We therefore examined whether Nav1.2 is expressed in of cells expressing GFP and found that Nav1.2 is not expressed in the axon initial segments (AISs) of GFP-positive cells in the cortex (Figure 3) and other brain regions (data not shown) further confirming the mutually-exclusive expression of Nav1.1 and Nav1.2.

Nav1.1 is expressed in pyramidal tract while Nav1.2 in cortico-striatal and cortico-thalamic projection neurons

We previously reported that a subpopulation of neocortical L5 pyramidal excitatory neurons are Nav1.1-positive (Ogiwara et al., 2013), but the nature of those neurons was unclear. A majority of neocortical excitatory projection neurons in L5 consist of pyramidal tract (PT) and intratelencephalic cortico-striatal (iCS) neurons, here we define iCS rather than CS because PT also occasionally innervate striatum, and those in L6 are mostly cortico-thalamic (CT) neurons (Shepherd, 2013). FEZ family zinc finger protein 2 transcriptional factor (FEZF2) is expressed in PT neurons which locate at L6 and form its axonal projection and regulates a decision between subcortical vs. callosal projection neuron fates (Chen et al., 2005; Chen et al., 2008), while a transcription T-box brain 1 transcription factor (TBR1), a negative regulator of FEZF2, is expressed in CT neurons which locate at L6 (Han et al., 2011; McKenna et al., 2011; Tantirigama et al., 2016). We therefore performed immunohistochemical investigations of Nav1.1-mimicing GFP signals in *Scn1a*-GFP mice by using FEZF2 and TBR1 as projection neuron markers (Figure 4 and Figure 5).

In all neocortical layers of *Scn1a*-GFP mice, cells with dense GFP signals are generally inhibitory interneurons (Supplemental Figure S1), and FEZF2 or TBR1 signals were found in cells with less intense GFP signals (see below) indicating that these are excitatory projection neurons.

In neocortical L5 of *Scn1a*-GFP mice where PT and iCS neurons are major populations (Shepherd, 2013), a majority of FEZF2-positive neurons are GFP-positive (~83% and ~98% of FEZF2-positive neurons in primary motor cortex are GFP-positive at P15 and 4-week-old, respectively) (Figure 4, Supplemental table S1). Consistently, a majority of GFP-positive neurons are TBR1-negative (only ~10% and ~4% of GFP-positive neurons in primary motor cortex are TBR1-positive at P15 and 4-week-old, respectively) (Figure 5 and 6, Supplemental table S1). Instead, most AISs of TBR1-positive neurons are Nav1.2-positive (Supplemental figure S2). Because a majority of L5 projection neurons consist of PT and iCS neurons

(Shepherd, 2013), these neurons are assumed to be iCS neurons. These results therefore indicate that in neocortical L5 PT neurons express Nav1.1 and iCS neurons express Nav1.2.

In neocortical L6 of *Scn1a*-GFP mice where CT and iCS neurons are major populations (Shepherd, 2013), a majority of TBR1-positive neurons are GFP-negative (~15% and ~26% of TBR1-positive neurons in primary motor cortex are GFP-positive at P15 and 4-week-old, respectively) (Figure 5 and 6, Supplemental table S1), indicating that CT neurons express Nav1.2.

In neocortical L2/3 of *Scn1a*-GFP mice where cortico-cortical (CC) neurons is a major population (Shepherd, 2013), a majority of TBR1-positive cells are GFP-positive and mostly half of GFP-positive cells are TBR1-positive (Figure 5 and 6, Supplemental table S1). These results indicate that a subpopulation of L2/3 CC neurons express Nav1.1, which is well consistent to the previous observation that Nav1.1 is expressed in callosal axons of neocortical excitatory neurons (Ogiwara et al., 2013). Because a majority of the L2/3 GFP/TBR1 double-positive neurons locate at L3, and because L3 CC neurons has been shown to target PT neurons (Anderson et al., 2010), the Nav1.1/TBR1 double-positive L3 CC neurons may possibly innervate PT (Figure 6). Because of intense Nav1.2 expressions are observed in AISs of many neurons at all neocortical layers including L2/3 (Yamagata et al., 2017), the remained Nav1.1-negative L2/3 CC neurons are assumed to be Nav1.2-positive (Figure 6).

Discussion

In the neocortex of juvenile and adult mouse brain, Nav1.2 is dominantly expressed in excitatory while Nav1.1 is dominant in inhibitory neurons (see Introduction), but Nav1.1 has also been suggested to be expressed in a subpopulation of excitatory neurons (Ogiwara et al., 2013). Here in the present study, we showed that among neocortical excitatory projection neurons Nav1.1 is expressed in PT and a subpopulation of CC neurons while Nav1.2 is expressed in iCS, CT and a distinct subpopulation of CC neurons (Figure 6). These findings should contribute to the elucidation of neural circuits responsible for diseases such as epilepsy and neurodevelopmental disorders caused by *SCN1A* and *SCN2A* mutations. For example, we previously reported that impaired excitatory neurotransmission of cortico-striatal fast-spiking inhibitory neurons (FSIs) neocortical projection neurons causes epilepsies in *Scn2a* haplodeficient mouse (Miyamoto et al., 2019). Our present finding of Nav1.2 expression in iCS neurons and Nav1.1 in PT neurons together with the previous finding that striatal direct and indirect-pathway medium spiny neurons (dMSNs and iMSNs) are predominantly targeted by IT and PT neurons, respectively (Lei et al., 2004), further refines this pathological circuit, in

which the hyperactivation of iMSNs is guaranteed by the intact excitatory input from Nav1.1-positive PT neurons and the decrease of Nav1.2-positive iCS excitatory input onto dMSN may decrease its suppression onto substantia nigra pars reticulata/ internal globus pallidus (SNr/GPi) in $Scn2a^{+/-}$ mouse, and both of these would contribute to the over-suppression onto thalamus. Because $SCN2A$ has been well established as one of top genes to show most frequent de novo loss-of-function mutations in patients with autism spectrum disorder (ASD) (Hoischen et al., 2014; Johnson et al., 2016) and because impaired striatal function was suggested in multiple ASD animal models (Fuccillo et al., 2016), the Nav1.2 expression in iCS neurons may contribute to understanding of the neural circuit for ASD as well. The finding of Nav1.1 expression in PT and CC neurons should also be useful, especially that in PT neurons now elucidates the pathological neural circuit for sudden unexpected death in epilepsy (SUDEP) of Dravet syndrome.

Dravet syndrome is a sporadic intractable epileptic encephalopathy characterized by early onset (6 months ~ 1 year after birth) epileptic seizures which firstly appear as febrile but later could be afebrile, intellectual disability, autistic features, ataxia and increased risk of SUDEP, and de novo loss-of-function mutations of $SCN1A$ are found in more than 80% of the patients (Claes et al., 2001; Sugawara et al., 2002; Fujiwara et al., 2003; Dravet et al., 2005; Depienne et al., 2009; Meng et al., 2015). In mice, loss-of-function $Scn1a$ mutations caused clinical features reminiscent of Dravet syndrome, including early-onset epileptic seizures, lowered threshold for hyperthermia-induced seizures, premature sudden death, hyperactivity, learning and memory deficits, reduced sociability and ataxic gaits (Yu et al., 2006; Ogiwara et al., 2007; Oakley et al., 2009; Cao et al., 2012; Han et al., 2012; Kalume et al., 2013; Ito et al., 2013).We and others have shown that Nav1.1 is densely localized at AISs of inhibitory cells such PV-IN (Ogiwara et al., 2007; Ogiwara et al., 2013; Li et al., 2014; Tai et al., 2014) and that selective elimination of Nav1.1 in PV-IN in mice caused a reduction of the gross amount of brain Nav1.1 by half, and resulted in epileptic seizures, sudden death and deficits in social behavior and spatial memory (Ogiwara et al., 2013; Tatsukawa et al., 2018). It is thus plausible that Nav1.1 haplo-deficiency in PV-IN play a pivotal role in the pathophysiology of many clinical aspects of Dravet syndrome.

Interestingly, mice with selective Nav1.1 haplo-elimination in global inhibitory neurons were at a greater risk of lethal seizure than constitutive Nav1.1 haplo-deficient mice, and the mortality risk of mice with Nav1.1 haplo-deficiency in inhibitory neurons was significantly decreased or improved with additional Nav1.1 haplo-elimination in dorsal telencephalic excitatory neurons, indicating beneficial effects of Nav1.1 deficient excitatory neurons in

seizure symptoms (Ogiwara et al., 2013). These facts indicate that although loss of function of inhibitory neurons is responsible for the sudden death in epilepsy, a part of excitatory neurons in the dorsal telencephalon such as neocortex and hippocampus could also contribute to aggravation of, or in other words becoming half amount of Nav1.1 in dorsal telencephalic excitatory neurons is ameliorating for, the disease symptoms in patients with Dravet syndrome. Because of the absence of Nav1.1 in hippocampal excitatory neurons (Ogiwara et al., 2007; 2013; Yamagata et al., 2017, and the present study), the ameliorating effect for epilepsy and sudden death was most possibly caused by Nav1.1 haploinsufficiency in neocortical excitatory neurons.

Kalume and colleagues (2013) reported that sudden death in Nav1.1 haplo-deficient mice occurred immediately after generalized tonic-clonic seizures and ictal bradycardia or slower heart rate, that the cardiac and sudden death phenotypes were reproduced in mice with forebrain GABAergic neuron-specific, but not cardiac neuron-specific heterozygous elimination of *Scn1a*, and that the ictal bradycardia and sudden death were suppressed by atropine, a competitive antagonist for muscarinic acetylcholine receptors, and therefore counteracts against parasympathetic nervous system. N-methyl scopolamine, a muscarinic receptor antagonist that does not cross the blood-brain barrier, also eliminated the bradycardia, and peripheral blockade of muscarinic receptors was therefore sufficient to reduce sudden death in the mice. These results indicated that epileptic seizures cause parasympathetic hyperactivity, which then cause ictal bradycardia and finally result in seizure-associated sudden death in the Nav1.1 haplo-deficient mice (Kalume et al., 2013).

Here in this study we revealed that Nav1.1 is expressed in PT neurons. Together with the above mentioned parasympathetic hyperactivity (Kalume et al., 2013) and the ameliorating effect of Nav1.1 haploinsufficiency in neocortical excitatory excitatory neurons (Ogiwara et al., 2013) observed in the sudden death of Nav1.1 haplo-deficient mice, the pathological neural circuit was assumed to be as follows, "Nav1.1 haploinsufficiency in neocortical PV-IN fails to suppress and therefore activates PT neurons as well as subsequent parasympathetic neurons and consequently suppresses heart activity and results in cardiac arrest" (Figure 7), in which Nav1.1 is remained in full amount in PT neurons of the mice with inhibitory neurons-specific haplo-elimination of Nav1.1 and therefore the lethality of the mice was further aggravated. To confirm this hypothetical circuit, further studies are required such as figuring-out the entities of Nav channels in pre-and post-ganglionic parasympathetic neurons and investigations of actual electrophysiological changes of each neuron in the circuit in Nav1.1 haplo-deficient mice.

Materials and Methods

Animal work statement

All animal experimental protocols were approved by the Animal Experiment Committee of Nagoya City University and RIKEN Center for Brain Science. Mice were handled in accordance with the guidelines of the Animal Experiment Committee.

Mice

Scn1a-GFP BAC transgenic mice were generated as follows. A murine BAC clone RP23-232A20 containing the *Scn1a* locus was obtained from the BACPAC Resource Center (https://bacpacresources.org). A GFP reporter cassette, comprising a red-shifted variant GFP cDNA and a downstream polyadenylation signal derived from pIRES2-EGFP (Takara Bio), was inserted in-frame into the initiation codon of the *Scn1a* coding exon 1 using the Red/ET Recombineering kit (Gene Bridges), according to the manufacturer's instructions. A correctly modified BAC clone verified using PCR and restriction mapping was digested with *Sac*II, purified using CL-4B sepharose (GE Healthcare), and injected into pronuclei of C57BL/6J zygotes. Mice carrying the BAC transgene were identified using PCR with primers: m*Scn1a*_TG_check_F1, 5'-TGTTCTCCACGTTTCTGGTT-3', m*Scn1a*_TG_check_R1, 5'-TTAGCCTTCTCTTCTGCAATG-3' and EGFP_R1, 5'-GCTCCTGGACGTAGCCTTC-3' that detect the wild-type *Scn1a* allele as an internal control (186 bp) and the inserted transgene (371 bp). Of fifteen independent founder lines that were crossed with C57BL/6J mice, twelve lines successfully transmitted the transgene to their progeny. Of twelve founders, two lines (#184 and 233) that display much stronger green fluorescent intensity compared with other lines were selected, and maintained on a congenic C57BL/6J background. The mouse lines had normal growth and development. #233 line has been deposited to the RIKEN BioResource Center (https://web.brc.riken.jp/en/) for distribution under the registration number RBRC10241.

Western blot analysis

5-week-old mouse brains were isolated and homogenized in homogenization buffer [(0.32 M sucrose, 10 mM HEPES, 2 mM EDTA and 1× complete protease inhibitor cocktail (Roche Diagnostics), pH 7.4)], and centrifuged for 15 min at 1,000 *g*. The supernatants were next centrifuged for 30 min at 30,000 *g*. The resulting supernatants were designated as the cytosol fraction. The pellets were subsequently resuspended in lysis buffer (50 mM HEPES and 2 mM

EDTA, pH 7.4) and centrifuged for 30 min at 30,000 g. The resulting pellets, designated as the membrane fraction, were dissolved in 2 M Urea, 1× NuPAGE reducing agent (Thermo Fisher Scientific) and 1× NuPAGE LDS sample buffer (Thermo Fisher Scientific). The cytosol and membrane fractions were separated on the NuPAGE Novex Tris-acetate 3–8% gel (Thermo Fisher Scientific) or the PAG mini SuperSep Ace Tris-glycine 5–20% gel (FUJIFILM Wako Pure Chemical), and transferred to nitrocellulose membranes (Bio-Rad). Membranes were probed with the rabbit anti-Nav1.1 (250 ng/ml; IO1, Ogiwara et al., 2007), chicken anti-GFP (1:5,000; ab13970, Abcam) and mouse anti-β tubulin (1:10,000; T0198, Sigma-Aldrich) antibodies, and incubated with the horseradish peroxidase-conjugated goat anti-rabbit IgG (1:2,000; sc-2004, Santa Cruz Biotechnology), rabbit anti-chicken IgY (1:1,000; G1351, Promega) and goat anti-mouse IgG (1:5,000; W4011, Promega) antibodies. Blots were detected using the enhanced chemiluminescence reagent (PerkinElmer).

Histochemistry

2–8-week-old mice were deeply anesthetized, perfused transcardially with 4% paraformaldehyde (PFA) in PBS (10 mM phosphate buffer, 2.7 mM KCl, and 137 mM NaCl, pH 7.4) or periodate-lysine-4% PFA (PLP). Brains were removed from the skull and post-fixed. For fluorescent imaging, PFA-fixed brains were cryoprotected with 30% sucrose in PBS, cut in 30 μm sections, and mounted on glass slides. The sections on glass slides were treated with TrueBlack Lipofuscin Autofluorescence Quencher (Biotium) to reduce background fluorescence. For immunofluorescence, frozen sections (30 μm) were incubated in 10mM citrate acid, pH 6.0, and 1mM EDTA, pH 8.0, for 20 min at 100 ℃, blocked with 4% BlockAce (DS Pharma Biomedical) in PBS for 1 hour at room temperature (RT), and incubated with the rabbit anti-Nav1.1 antibody (250 ng/ml; IO1, Ogiwara et al. 2007) for 3 overnights (~50 hr) at RT. To detect GFP, ankyrin G, parvalbumin and somatostatin, the sections were incubated with the rat anti-GFP (1:500; GF090R, Nacalai Tesque), goat ankyrin G antibody (SC-12719, Santa Cruz Biotechnology), mouse anti-parvalbumin (1:30,000; 235, Swant) , rabbit anti-parvalbumin (1:5,000; PC255L, Merck), rabbit anti-somatostatin (1:200; AB5494, Merck-Millipore), rabbit anti-somatostatin (1:5,000; T-4103, Peninsula Laboratories), goat anti-somatostatin (1:5,000; SC-31778, Santa Cruz Biotechnology) antibodies. The sections were then incubated with the secondary antibodies conjugated with Alexa Fluor 488, 594, and 647 (1:1,000; Thermo Fisher Scientific), biotin (1:200; Vector Laboratories), or DyLight 488 and 649 (1:500; Jackson ImmunoResearch). The biotinylated antibody was visualized with streptavidin conjugated with Alexa Fluor 594 or 647 (1:1,000; Thermo Fisher Scientific). For immunofluorescent staining

in Figure 3-5, we prepared 6 μm sections from paraffin embedded PLP-fixed brains. The sections were processed as previously described (Yamagata et al., 2017). Following antibodies were used to detect GFP, Nav1.2, TBR1, FEZF2, and Ankyrin G; mouse anti-GFP antibodies (1:500; 11814460001, Roche Diagnostics), rabbit anti-Nav1.2 antibody (1:1,000; ASC-002, Alomone Labs), rabbit anti-TBR1 antibody (1:1,000; ab31940, Abcam or 1:500; SC-376258, Santa Cruz Biotechnology), rabbit anti-FEZF2 antibody (1:500; #18997, IBL), and goat ankyrin G antibody (1:500; SC-12719, Santa Cruz Biotechnology). As a secondary antibody, Alexa Fluor Plus 488 and 594 conjugated antibodies (1:1,000; A32723; A32754; Thermo Fisher Scientific) were used. Images were captured using a confocal laser scanning microscope (TCS SP2, Leica Microsystems) and fluorescence microscopes (BZ-8100 and BZ-X710, Keyence), and processed with Adobe Photoshop Elements 10 (Adobe Systems) and BZ-X analyzer (Keyence). Fluorescent cells were counted using BZ-X analyzer (Keyence), and the percentage of GFP-positive cells co-labeled for Nav1.2, TBR1, or FEZF2 were determined for each mouse. Data represent the mean ± standard error of the mean (SEM).

In situ hybridization.

Frozen sections (30 μm) of PFA-fixed mouse brains at P28 were incubated in 0.3% H_2O_2 in PBS for 30 min at RT to quench endogenous peroxidases, and mounted on glass slides. The sections on slides were UV irradiated with 1,250 mJ/cm^2 (Bio-Rad), permeabilized with 0.3% TritonX-100 in PBS for 15 min at RT, and digested with 1 μg/ml proteinase K (Nacalai Tesque) in 10mM Tris-HCl and 1mM EDTA, pH 8.0, for 30 min at 37°C, washed twice with 100 mM glycine in PBS for 5 min at RT, fixed with 4 % formaldehyde in PBS for 5 min at RT, and acetylated with 0.25% acetic anhydride in 100 mM triethanolamine, pH8.0. After acetylation, the sections were washed twice with 0.1 M phosphate buffer, pH 8.0, incubated in a hybridization buffer [(50% formamide, 5× SSPE, 0.1% SDS, and 1 mg/ml Yeast tRNA(Roche Diagnostics)] containing the Avidin solution (Vector Laboratories) for 2 hr at 60°C, and hybridized with 2 μg/ml digoxigenin (DIG)- and dinitrophenol (DNP)-labeled probes in a hybridization buffer containing the Biotin solution (Vector Laboratories) overnight at 60°C in a humidified chamber. The hybridized sections were washed twice with 50% formamide in 2× SSC for 15 min at 50°C, incubated in TNE (1 mM EDTA, 500 mM NaCl, 10 mM Tris-HCl, pH 8.0) for 10 min at 37°C, treated with 20 μg/ml RNase A (Nacalai Tesque) in TNE for 15 min at 37°C, washed 2× SSC twice for 15 min each at 37°C twice and 0.2× SSC twice for 15 min each at 37°C. After washing twice in a high stringency buffer (10 mM Tris, 10 mM EDTA and 500

mM NaCl, pH 8.0) for 10 min each at RT, the sections were blocked with a blocking buffer [20 mM Tris and 150 mM NaCl, pH 7.5 containing 0.05% Tween-20, 4% BlockAce (DS Pharma Biomedical) and 0.5× Blocking reagent (Roche Diagnostics)] for 1 hr at RT, and incubated with the alkaline phosphatase-conjugated sheep anti-DIG (1:500; 11093274910, Roche Diagnostics) and biotinylated rabbit anti-DNP (1:100; BA-0603, Vector laboratories) antibodies in a blocking buffer overnight at 4°C, followed by incubation with the biotinylated goat anti-rabbit antibody (1:200; BA-1000, Vector laboratories) in a blocking buffer at RT for 1 to 2hr. The probes were visualized using the NBT/BCIP kit (Roche Diagnostics), VECTASTAIN Elite ABC kit (Vector laboratories) and ImmPACT DAB substrate (Vector laboratories).

The DIG-labeled RNA probes for *Scn1a* designed to target the 3'-untranlated region (nucleotides 6,488–7,102 from accession number NM_001313997.1) were described previously (Ogiwara et al., 2007), and synthesized using the MEGAscript transcription kits (Thermo Fisher Scientific) with DIG-11-UTP (Roche Diagnostics). The DNP-labeled RNA probes for GFP were derived from the fragment corresponding to nucleotides 1,256–1,983 in pIRES2-EGFP (Takara Bio), and prepared using the MEGAscript transcription kits (Thermo Fisher Scientific) with DNP-11-UTP (PerkinElmer).

**Competing interests**

No competing interests declared.

References

1. Anderson CT, Sheets PL, Kiritani T, Shepherd GM. Sublayer-specific microcircuits of corticospinal and corticostriatal neurons in motor cortex. *Nat. Neurosci.* **13**(6):739-744 (2010).

2. Cao, D., Ohtani, H., Ogiwara, I., Ohtani, S., Takahashi, Y., Yamakawa, K., Inoue, Y. Efficacy of stiripentol in hyperthermia-induced seizures in a mouse model of Dravet syndrome. *Epilepsia* **53**, 1140-1145 (2012).

3. Catterall WA. Voltage-gated sodium channels at 60: structure, function and pathophysiology. *J. Physiol.* **590**(11):2577-2589 (2012).

4. Chen B, Schaevitz L.R., McConnell S.K. Fezl regulates the differentiation and axon targeting of layer 5 subcortical projection neurons in cerebral cortex. *Proc. Natl. Acad. Sci. USA* **102**:17184–17189 (2005).

5. Chen B, Wang SS, Hattox AM, Rayburn H, Nelson SB, McConnell SK. The Fezf2-Ctip2 genetic pathway regulates the fate choice of subcortical projection neurons in the developing cerebral cortex. *Proc. Natl. Acad. Sci. USA*. **105**(32):11382-11387 (2008).

6. Claes, L., Del-Favero, J., Ceulemans, B., Lagae, L., Van Broeckhoven, C., De Jonghe, P. De novo mutations in the sodium-channel gene *SCN1A* cause severe myoclonic epilepsy of infancy. *Am. J. Hum. Genet.* **68,** 1327–1332 (2001).

7. Depienne, C., Trouillard, O., Saint-Martin, C., Gourfinkel-An, I., Bouteiller, D., Carpentier, W., Keren, B., Abert, B., Gautier, A., Baulac, S., Arzimanoglou, A., Cazeneuve, C., Nabbout, R., LeGuern, E. Spectrum of *SCN1A* gene mutations associated with Dravet syndrome: analysis of 333 patients. *J. Med. Genet.* **46**, 183–191 (2009).

8. Dravet, C., Bureau, M., Oguni, H., Fukuyama, Y. & Cokar, O. Severe myoclonic epilepsy in infancy (Dravet syndrome) in *Epileptic Syndromes in Infancy, Childhood and Adolescence, 4th edn* (eds. Roger, J. *et al.*) 89–113 (John Libbey Eurotext Ltd, Montrouge, France, 2005).

9. Fuccillo MV. Striatal Circuits as a Common Node for Autism Pathophysiology. *Front. Neurosci.* **10**:27 (2016).

10. Fujiwara, T., Sugawara, T., Mazaki-Miyazaki, E., Takahashi, Y., Fukushima, K., Watanabe, M., Hara, K., Morikawa, T., Yagi, K., Yamakawa, K., Inoue, Y. Mutations of sodium channel α subunit type 1 (*SCN1A*) in intractable childhood epilepsies with frequent generalized tonic-clonic seizures. *Brain* **126**, 531–546 (2003).

11. Goff, K. M., Goldberg, E.M. Vasoactive intestinal peptide-expressing interneurons are

impaired in a mouse model of Dravet syndrome. *Elife*. **8,** e46846; 10.7554/eLife.46846 (2019).

12. Han, S., Tai, C., Westenbroek, R. E., Yu, F. H., Cheah, C. S., Potter, G. B., Rubenstein, J. L., Scheuer, T., de la Iglesia, H. O., Catterall, W. A. Autistic-like behaviour in *Scn1a*$^{+/-}$ mice and rescue by enhanced GABA-mediated neurotransmission. *Nature* **489**, 385–390 (2012).

13. Han, W., Kwan, K.Y., Shim, S., Lam, M.M.S., Shin, Y., Xu, X., Zhu, Y., Li, M., Sestan, N. TBR1 directly represses Fezf2 to control the laminar origin and development of the corticospinal tract. *Proc. Natl. Acad. Sci. USA* **108**(7), 3041-3046 (2011)

14. Hoischen A, Krumm N, Eichler EE. Prioritization of neurodevelopmental disease genes by discovery of new mutations. *Nat. Neurosci*. **17**(6):764-772 (2014).

15. Ito, S., Ogiwara, I., Yamada, K., Miyamoto, H., Hensch, T. K., Osawa, M., Yamakawa, K. Mouse with Nav1.1 haploinsufficiency, a model for Dravet syndrome, exhibits lowered sociability and learning impairment. *Neurobiol. Dis.* **49**, 29–40 (2013).

16. Johnson MR, Shkura K, Langley SR, Delahaye-Duriez A, Srivastava P, Hill WD, Rackham OJ, Davies G, Harris SE, Moreno-Moral A, Rotival M, Speed D, Petrovski S, Katz A, Hayward C, Porteous DJ, Smith BH, Padmanabhan S, Hocking LJ, Starr JM, Liewald DC, Visconti A, Falchi M, Bottolo L, Rossetti T, Danis B, Mazzuferi M, Foerch P, Grote A, Helmstaedter C, Becker AJ, Kaminski RM, Deary IJ, Petretto E. Systems genetics identifies a convergent gene network for cognition and neurodevelopmental disease. *Nat. Neurosci*. **19**(2):223-232 (2016).

17. Kalume, F., Westenbroek, R.E., Cheah, C.S., Yu, F.H., Oakley, J.C., Scheuer, T., Catterall, W.A. Sudden unexpected death in a mouse model of Dravet syndrome. *J. Clin. Invest.* **123**, 1798–1808 (2013).

18. Lei W, Jiao Y, Del Mar N, Reiner A. Evidence for differential cortical input to direct pathway versus indirect pathway striatal projection neurons in rats. *J Neurosci*. **24**(38), 8289-8299, (2004).

19. Li, T., Tian, C., Scalmani, P., Frassoni, C., Mantegazza, M., Wang, Y., Yang, M., Wu, S., Shu, Y. Action potential initiation in neocortical inhibitory interneurons. *PLoS Biol.* **12,** e1001944; 10.1371/journal.pbio.1001944 (2014).

20. Lorincz A, Nusser Z. Cell-type-dependent molecular composition of the axon initial segment. *J. Neurosci*. **28**(53), 14329-14340 (2008).

21. Lorincz A, Nusser Z. Molecular identity of dendritic voltage-gated sodium channels. *Science* **328**(5980):906-909 (2010).

22. McKenna WL, Betancourt J, Larkin KA, Abrams B, Guo C, Rubenstein JL, Chen B. Tbr1

and Fezf2 regulate alternate corticofugal neuronal identities during neocortical development. *J. Neurosci*. **31**(2):549-564 (2011).

23. Meisler MH, Hill SF, Yu W. Sodium channelopathies in neurodevelopmental disorders. *Nat. Rev. Neurosci*. **22**(3):152-166 (2021).

24. Meng, H., Xu, H.Q., Yu, L., Lin, G.W., He, N., Su, T., Shi, Y.W., Li, B., Wang, J., Liu, X.R., Tang, B., Long, Y.S., Yi, Y.H., Liao, W.P. The *SCN1A* mutation database: updating information and analysis of the relationships among genotype, functional alteration, and phenotype. *Hum. Mutat*. 36, 573–580 (2015).

25. Miyamoto H, Tatsukawa T, Shimohata A, Yamagata T, Suzuki T, Amano K, Mazaki E, Raveau M, Ogiwara I, Oba-Asaka A, Hensch TK, Itohara S, Sakimura K, Kobayashi K, Kobayashi K, Yamakawa K. Impaired cortico-striatal excitatory transmission triggers epilepsy. *Nat. Commun*. **10**(1):1917 (2019).

26. Nakayama T, Ogiwara I, Ito K, Kaneda M, Mazaki E, Osaka H, Ohtani H, Inoue Y, Fujiwara T, Uematsu M, Haginoya K, Tsuchiya S, Yamakawa K. Deletions of SCN1A 5' genomic region with promoter activity in Dravet syndrome. *Hum. Mutat*. **31**(7):820-829 (2010).

27. Oakley, J.C., Kalume, F., Yu, F.H., Scheuer, T. Catterall, W.A. Temperature- and age-dependent seizures in a mouse model of severe myoclonic epilepsy in infancy. *Proc. Natl. Acad. Sci. USA* **106**, 3994–3999 (2009).

28. Ogiwara, I., Miyamoto, H., Morita, N., Atapour, N., Mazaki, E., Inoue, I., Takeuchi, T., Itohara, S., Yanagawa, Y., Obata, K., Furuichi, T., Hensch, T.K., Yamakawa, K. Nav1.1 Localizes to axons of parvalbumin-positive inhibitory interneurons: A circuit basis for epileptic seizures in mice carrying an *Scn1a* gene mutation. *J. Neurosci*. **27**, 5903–5914 (2007)

29. Ogiwara, I., Iwasato, T., Miyamoto, H., Iwata, R., Yamagata, T., Mazaki, E., Yanagawa, Y., Tamamaki, N., Hensch, T.K., Itohara, S., Yamakawa, K. Nav1.1 haploinsufficiency in excitatory neurons ameliorates seizure-associated sudden death in a mouse model of Dravet syndrome. *Hum. Mol. Genet*. **22**, 4784–4804 (2013).

30. Ogiwara I, Miyamoto H, Tatsukawa T, Yamagata T, Nakayama T, Atapour N, Miura E, Mazaki E, Ernst SJ, Cao D, Ohtani H, Itohara S, Yanagawa Y, Montal M, Yuzaki M, Inoue Y, Hensch TK, Noebels JL, Yamakawa K. Nav1.2 haplodeficiency in excitatory neurons causes absence-like seizures in mice. *Commun.. Biol*. **1**:96 (2018).

31. Shepherd GM. Corticostriatal connectivity and its role in disease. *Nat. Rev. Neurosci*. **14**, 278-291 (2013).

32. Sugawara, T. *et al.* Frequent mutations of *SCN1A* in severe myoclonic epilepsy in infancy.

Neurology **58**, 1122–1124 (2002).

33. Tai, T., Abe, Y., Westenbroek, R. E., Scheuer, T., Catterall, W. A. Impaired excitability of somatostatin- and parvalbumin-expressing cortical interneurons in a mouse model of Dravet syndrome. *Proc. Natl. Acad. Sci. USA* **111**, E3139–3148; 10.1073/pnas.1411131111 (2014).

34. Tantirigama ML, Oswald MJ, Clare AJ, Wicky HE, Day RC, Hughes SM, Empson RM. Fezf2 expression in layer 5 projection neurons of mature mouse motor cortex. *J. Comp. Neurol*. **524**, 829-845 (2016).

35. Tatsukawa, T., Ogiwara, I., Mazaki, E., Shimohata, A., Yamakawa, K. Impairments in social novelty recognition and spatial memory in mice with conditional deletion of *Scn1a* in parvalbumin-expressing cells. *Neurobiol. Dis.* **112**, 24–34 (2018).

36. Tian C, Wang K, Ke W, Guo H, Shu Y. Molecular identity of axonal sodium channels in human cortical pyramidal cells. *Front Cell Neurosci*. **8**: 297 (2014).

37. Yamagata, T., Ogiwara, I., Mazaki, E., Yanagawa, Y. & Yamakawa, K. Nav1.2 is expressed in caudal ganglionic eminence-derived disinhibitory interneurons: Mutually exclusive distributions of Nav1.1 and Nav1.2. *Biochem. Biophys. Res. Commun.* **491**, 1070–1076 (2017).

38. Yamakawa, K. Mutations of voltage-gated sodium channel genes *SCN1A* and *SCN2A* in epilepsy, intellectual disability, and autism in *Neuronal and synaptic dysfunction in autism spectrum disorder and intellectual disability* (eds. Sara, C. & Verpelli, C.) 233–251 (Elsevier, Amsterdam, Netherlands, 2016).

39. Yu, F. H. *et al.* Reduced sodium current in GABAergic interneurons in a mouse model of severe myoclonic epilepsy in infancy. *Nat. Neurosci.* **9**, 1142–1149 (2006).
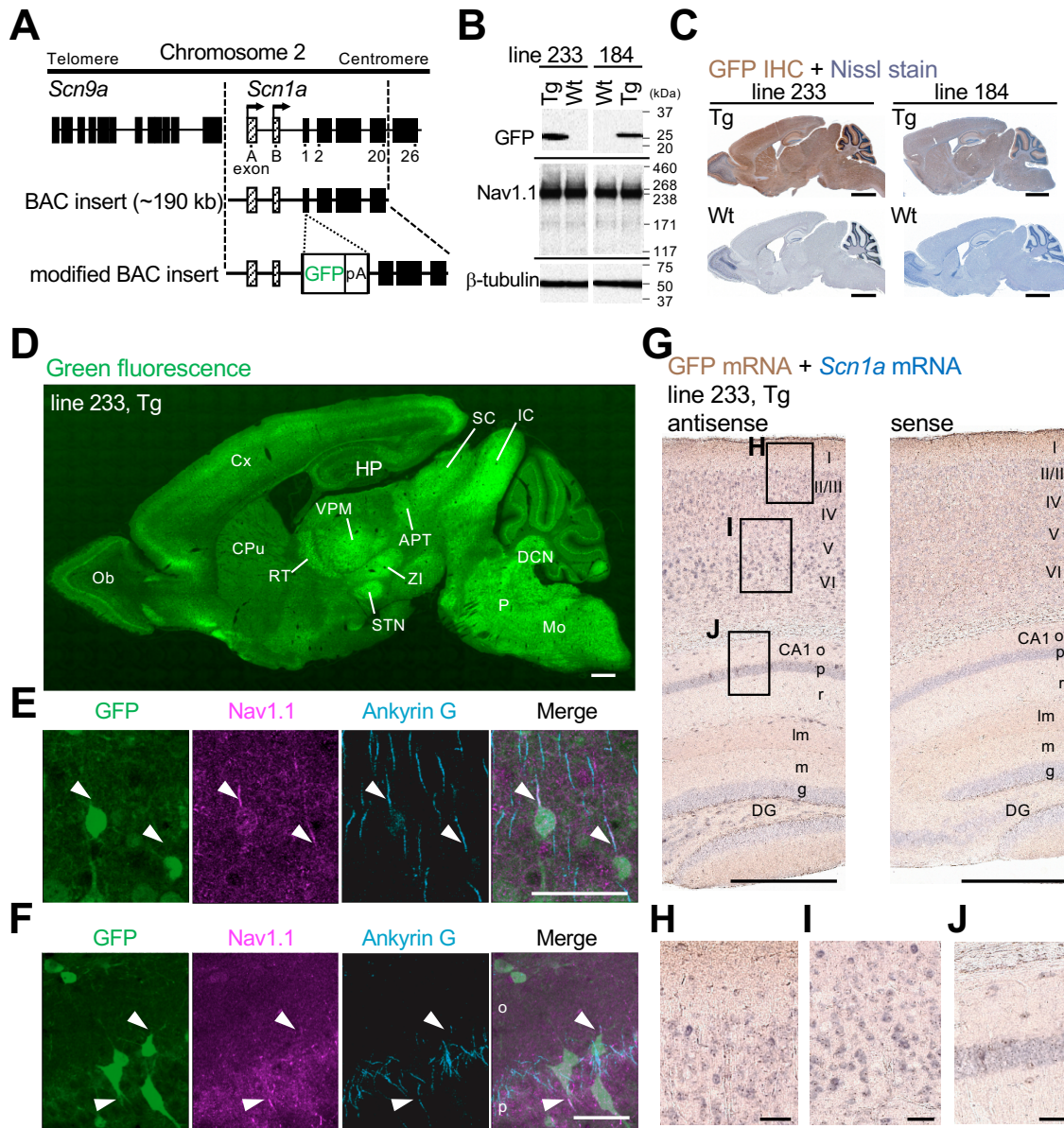
Figure 1. Generation and verification of *Scn1a*-GFP mice.

(A) Schematic representation of the modified BAC construct containing the *Scn1a*-GFP transgene. A GFP reporter cassette consisting of GFP cDNA and a polyadenylation signal was inserted at the ATG initiation codon in the coding exon 1 of *Scn1a*. Filled and hatched boxes indicate the coding and non-coding exons of *Scn9a* and *Scn1a*. Arrows indicate the start sites and orientation of transcription of *Scn1a*. **(B)** Western blot analysis for *Scn1a*-GFP and endogenous Nav1.1. The whole cytosolic and membrane fractions from 5-week-old *Scn1a*-GFP brains (#233 and #184 lines) were probed with anti-GFP and anti-Nav1.1 antibodies, respectively. β-Tubulin was used as an internal control. **(C)** Immunohistochemistry for *Scn1a*-GFP. Parasagittal sections from 5–6-week-old *Scn1a*-GFP brains (lines #233 and 184) were probed with anti-GFP antibody (red) and counterstained with Nissl stains labeling nuclei

(violet). **(D)** Fluorescent imaging for *Scn1a*-GFP. Parasagittal sections from 8-week-old *Scn1a*-GFP brains (line #233) exhibited bright green fluorescence. Ob, olfactory bulb; Cx, cerebral cortex; CPu, caudate putamen; RT, reticular thalamic nucleus; VPM, ventral posteromedial thalamic nucleus; HP, hippocampus; STN, subthalamic nucleus; ZI, zona incerta; APT, anterior pretectal nucleus; SC, superior colliculus; IC, inferior colliculus; DCN, deep cerebellar nuclei; P, pons; Mo, medulla oblongata. **(E, F)** Co-expression analysis of *Scn1a*-GFP and endogenous Nav1.1 using immunofluorescence histochemistry. Sagittal sections of cortex (E) and hippocampus (F) of P16.5 *Scn1a*-GFP brains (#233 line) were probed with anti-GFP (green), anti-Nav1.1 (magenta), and anti-ankyrin G (cyan) antibodies. Arrowheads indicate Nav1.1-immunoreactive AISs of GFP-expression cells. **(G-J)** Double *in situ* hybridization for *Scn1a*-GFP transgene mRNA and endogenous *Scn1a* mRNA. Parasagittal sections from P28 *Scn1a*-GFP brains (#233 line) were hybridized with sense (left) and antisense (right) RNA probes for GFP transgene (brown) and endogenous *Scn1a* (blue) mRNA species. CA, cornu ammonis; DG, dentate gyrus; o, stratum oriens; p, stratum pyramidale; r, stratum radiatum; lm, stratum lacunosum-moleculare, m, stratum moleculare; g, stratum granulosum. Magnified images outlined in (G) are shown in (H-J). Tg, hemizygous *Scn1a*-GFP transgenic mice; Wt, wild-type littermates. Representative images are shown. Scale bars; 500 μm (C, D, G), 50 μm (E, F, H-J).
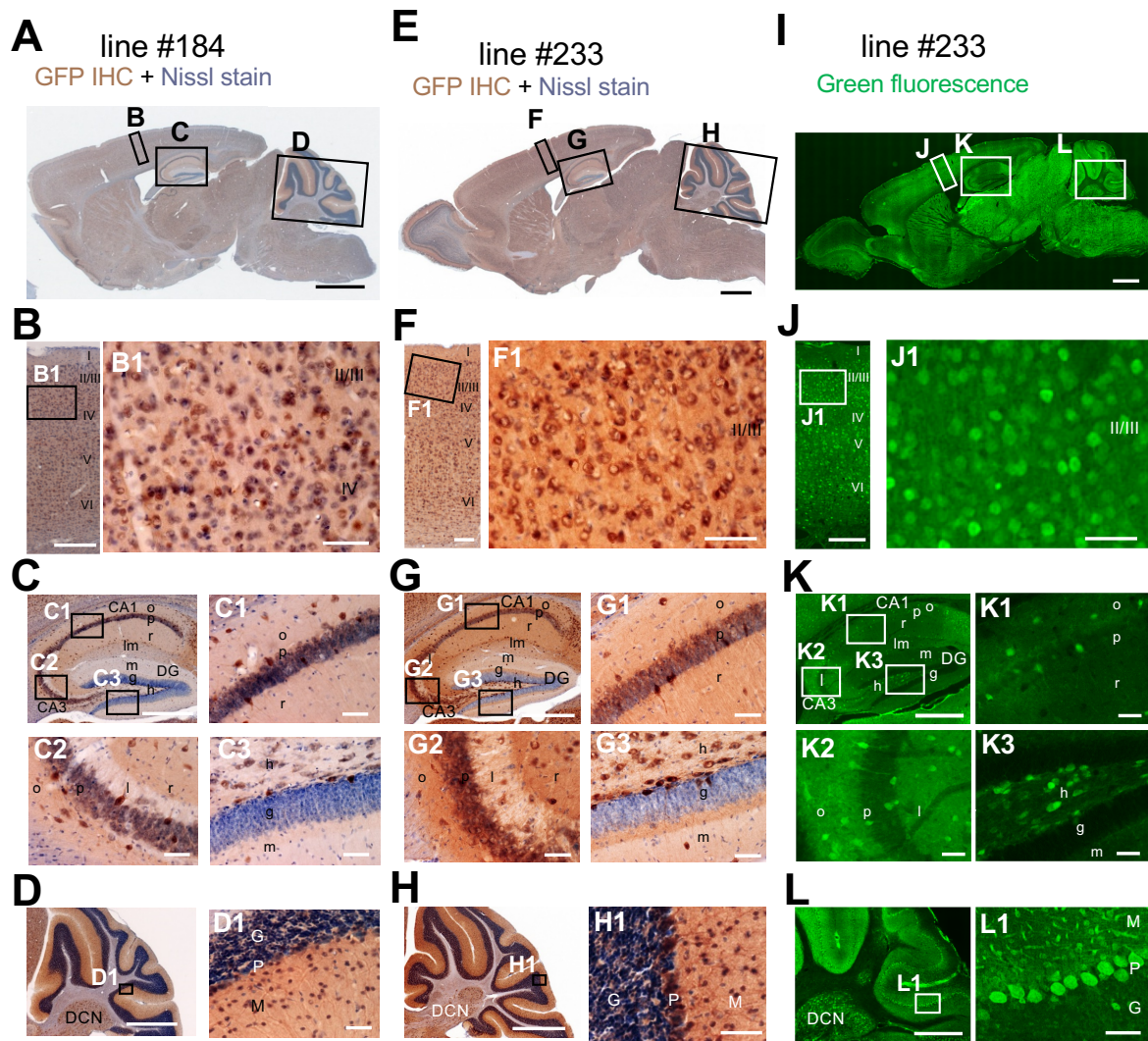
Figure 2. Distribution of GFP-expressing cells in *Scn1a*-GFP mouse brain.

Immunohistochemical images of parasagittal section from 5–6-week-old *Scn1a*-GFP brains (#184 and #233 line), showing GFP immunostaining (brown) with Nissl counterstaining (violet) in (**A-D)** and (**E-H)**, respectively. While #184 line apparently expressed GFP at a weaker intensity than #233 line, the two lines showed a similar distribution pattern of GFP-expressing cells across all brain regions. Fluorescent images of GFP (green) in parasagittal sections from 5–6-week-old *Scn1a*-GFP brains (#233 line) are shown in (**I-L)**. Higher-magnification images outlined in (A, E, I) are shown in (B-D, F-H, J-L). In neocortex (B, F, J), GFP-expressing cells were scattered throughout the entire region. Boxed areas in (B, F, J**)** are magnified in (B1, F1, J1). In hippocampus (C, G, K), GFP-positive inhibitory neurons were sparsely distributed in the CA fields and dentate gyrus, while excitatory neurons in stratum pyramidale and granulosum striatum are GFP-negative. Boxed areas in (C, G, K) are magnified in (C1-3, G1-

3, K1-3). In cerebellum (D, H, L), Purkinje, basket, and deep cerebellar nuclei cells were GFP-positive. Boxed areas in (D, H, L) are magnified in (D1, H1, L1). CA, cornu ammonis; DG, dentate gyrus; o, stratum oriens; p, stratum pyramidale; r, stratum radiatum; lm, stratum lacunosum-moleculare; l, stratum lucidum; m, stratum moleculare; g, stratum granulosum; h, hilus; DCN, deep cerebellar nuclei; M, molecular layer; P, Purkinje cell layer; G, granular cell layer. Scale bars; 1 mm (A, E, J), 500 μm (B-D, F-H, J-L), 50 μm (B1, C1-3, D1, F1, G1-3, H1, J1, K1-3, L1).
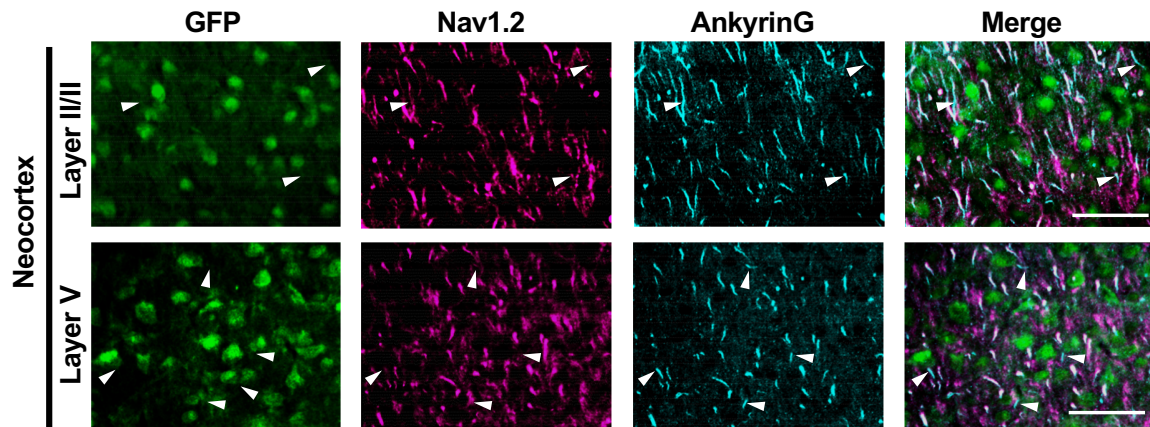
Figure 3. AISs of GFP-positive cell are Nav1.2-negative in *Scn1a*-GFP mouse neocortex.
Immunofluorescence images of neocortical L2/3 and L5 of *Scn1a*-GFP mice (#233 line) at P15 stained by mouse anti-GFP (green), rabbit anti-Nav1.2 (magenta), and goat anti-ankyrin G (cyan) antibodies. Note that AISs of GFP-positive cell are Nav1.2-negative (arrowheads). Scale bars: 50μm.
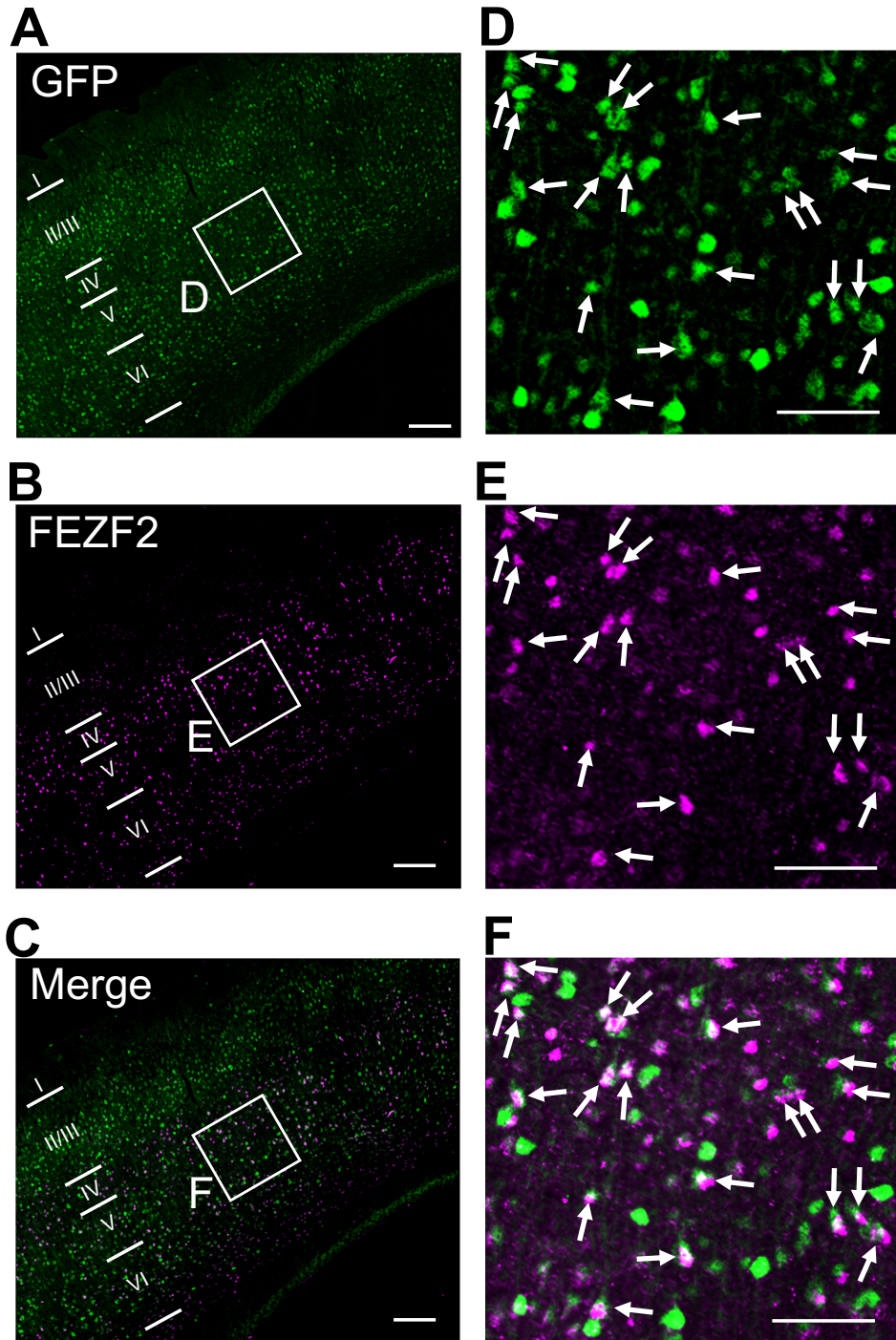
Figure 4. Most of FEZF2-positive cells are GFP (Nav1.1)-positive at L5 of *Scn1a*-GFP mouse neocortex.

(A-F) Distribution of GFP and FEZF2 immunosignals in neocortex of *Scn1a*-GFP mouse (#233 line) at 4-week-old detected by mouse anti-GFP (green) and rabbit anti-FEZF2 (magenta) antibodies. Arrows indicate GFP /FEZF2-double positive cells. Higher-magnified images outlined in (A, B, C) are shown in (D, E, F). Note that FEZF2 signals mostly overlap with GFP signals in L5. Many of the remained GFP-positive/FEZF2-negative cells have intense GFP

signals and are assumed to be inhibitory neurons. Scale bars: (A-C) 100μm. Scale bars: (E-F) 50μm.
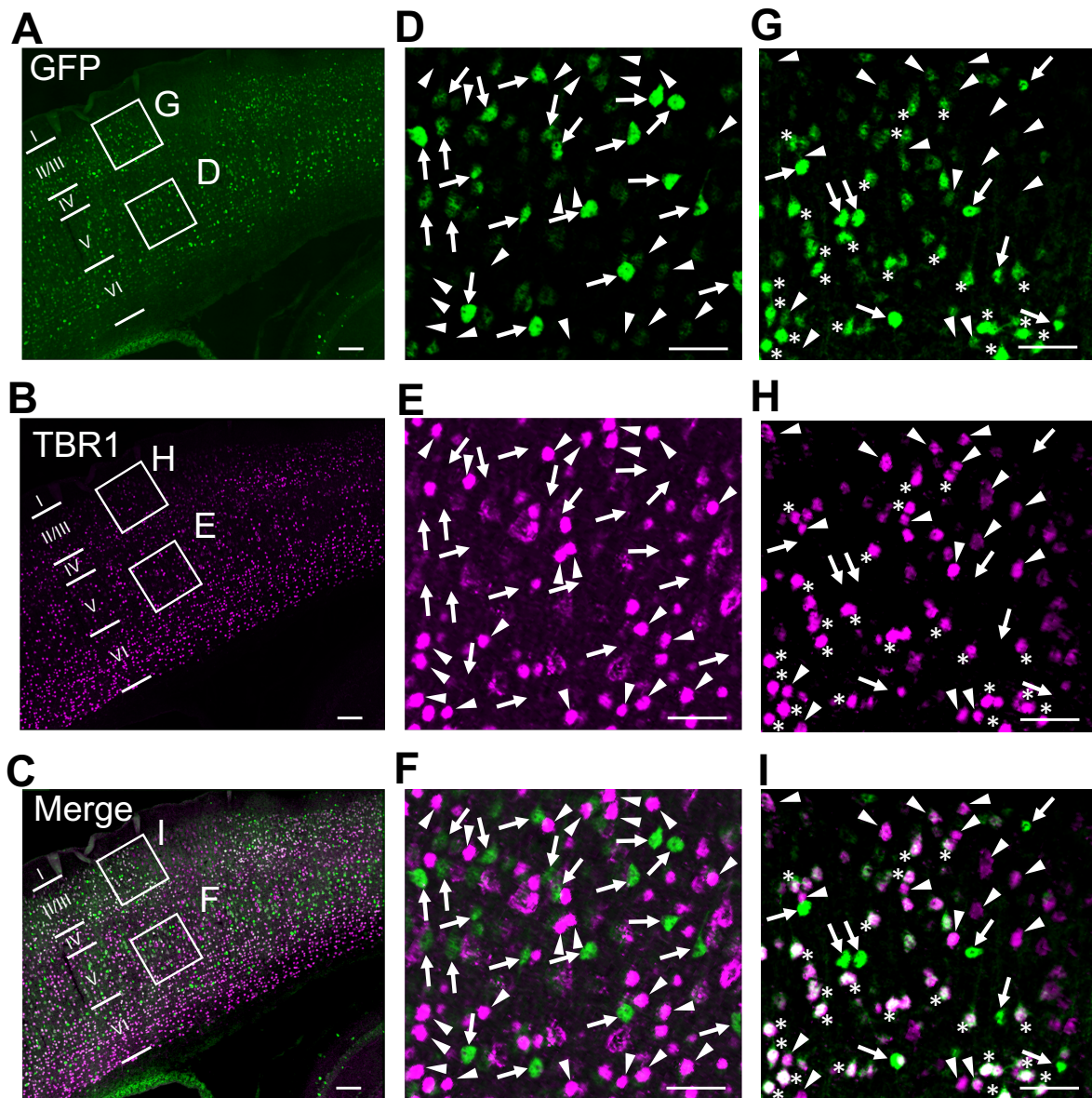
Figure 5. GFP (Nav1.1)-positive cells were mostly TBR1-negative at L5/6 but largely positive at L3 of *Scn1a*-GFP mouse neocortex.

(**A-I**) Distribution of GFP and TBR1 immunosignals in neocortex of *Scn1a*-GFP mouse (#233 line) at 4-week-old detected by mouse anti-GFP (green) and rabbit anti-TBR1 (magenta) antibodies. Arrows indicate GFP-positive/TBR1-negative cells. Arrowheads indicate TBR1-positive/GFP-negative cells. Asterisks (＊) indicate CFP/TBR1-double positive cells. Higher-magnified images outlined in (A, B, C) are shown in (D, E, F, G, H, I). Note that at L5/6 GFP-positive cells were mostly TBR1-negative but at L3 a major population of GFP-positive cells are TBR1-positive. Scale bars: (A-C) 100µm. Scale bars: (E-I) 50µm.
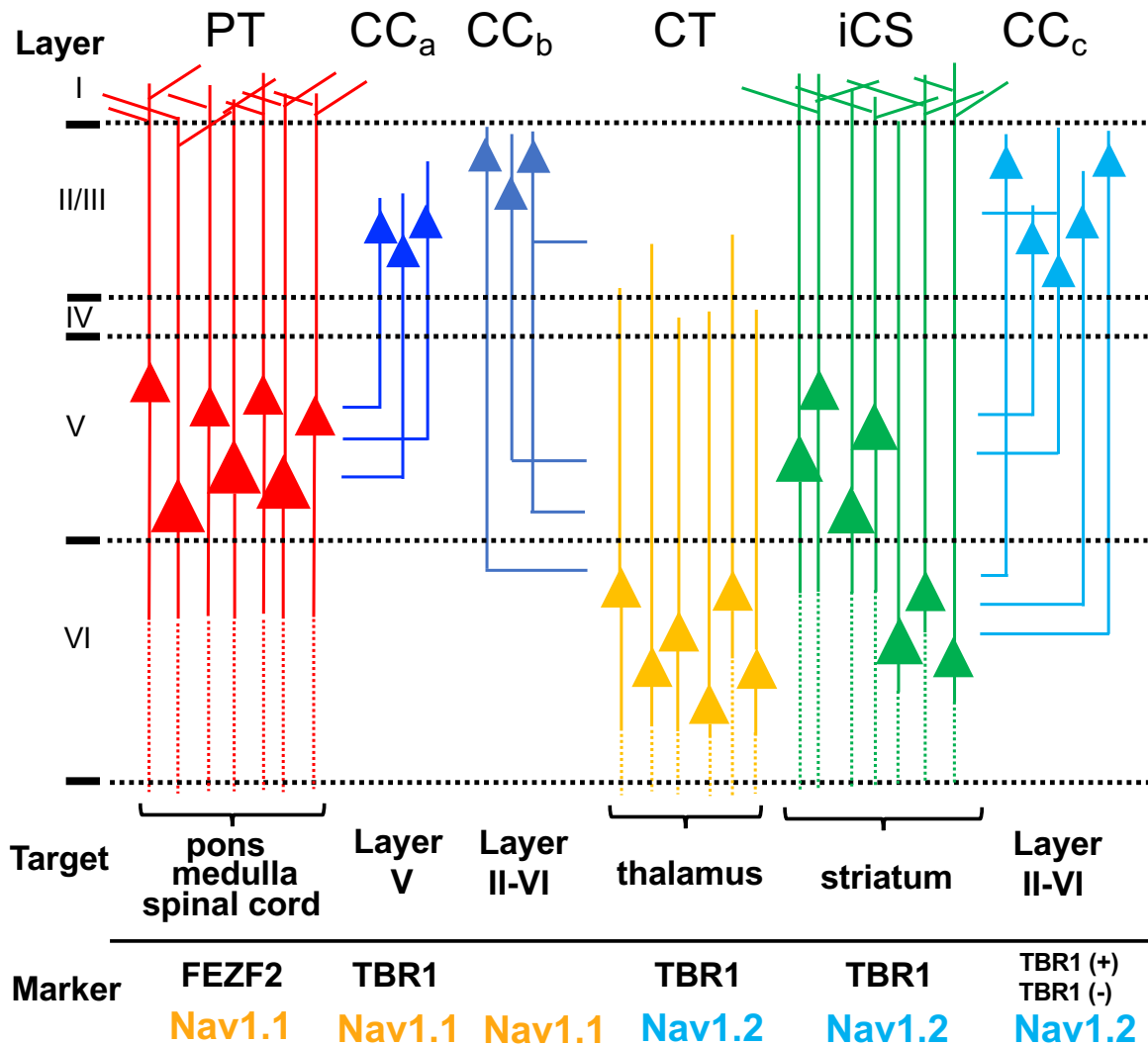
Figure 6. Nav1.1 and Nav1.2 distributions among neocortical projection neurons.
Nav1.1 is expressed in PT, CCa, CCb, while Nav1.2 is expressed in CT, iCS and CCc neocortical projection neurons. A subpopulation of CCc neurons are TBR1-positive, and most of those are assumed to be FEZF2-negative because of the paucity of cells with FEZF2 signals in L2/3. PT: pyramidal tract projection neurons. CCa, CCb, CCc: cortico-cortical projection neuron subpopulations. iCS: intratelencephalic cortico-striatal projection neurons. CT: cortico-thalamic projection neurons.
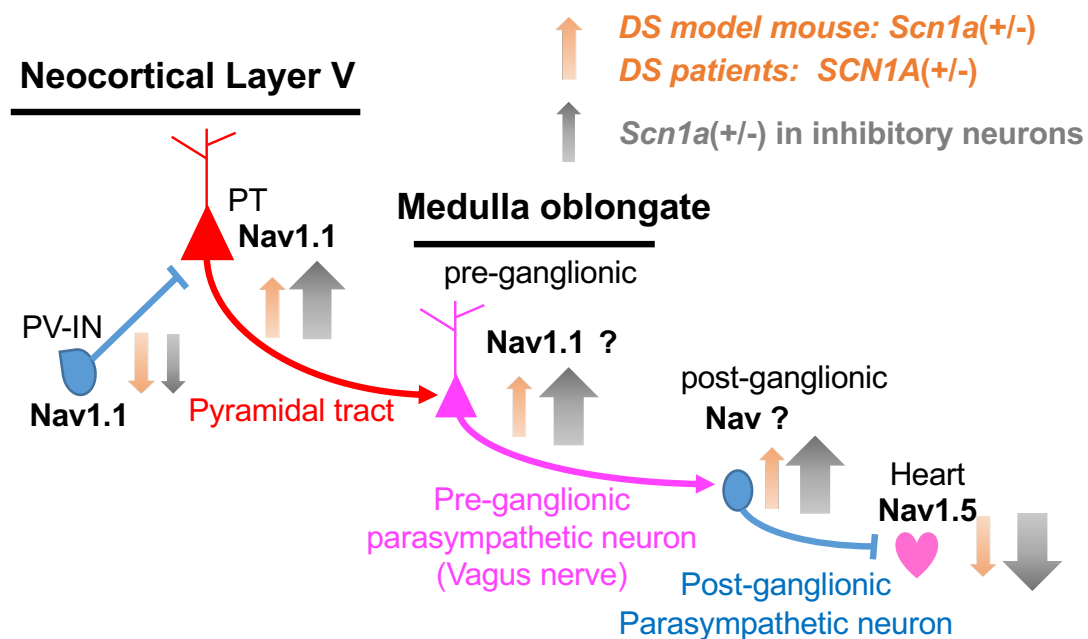
Figure 7. Hypothetical neural circuit for sudden death in *Scn1a*$^{+/-}$ mouse

In the Dravet syndrome model mouse *Scn1a*$^{+/-}$, Nav1.1 haploinsufficiency in neocortical parvalbumin-positive inhibitory neurons (PV-IN) disinhibits, or fails to suppress, and therefore activates neocortical layer V pyramidal tract projection neurons (PT) and successive parasympathetic neurons, pre-ganglionic and post-ganglionic vagus nerve, and suppresses heart activity and consequently results in cardiac arrest. In the mouse with inhibitory neuron-specific Nav1.1 haploinsufficiency (Ogiwara et al., 2013), PV-IN activity is decreased same to that of *Scn1a*$^{+/-}$ but Nav1.1 in PT neurons remained same to that of wild-type mouse and therefore the levels of hyperactivity of PT neurons and suppression of heart are farther increased and results in the severer epileptic seizures and sudden death in the mice.
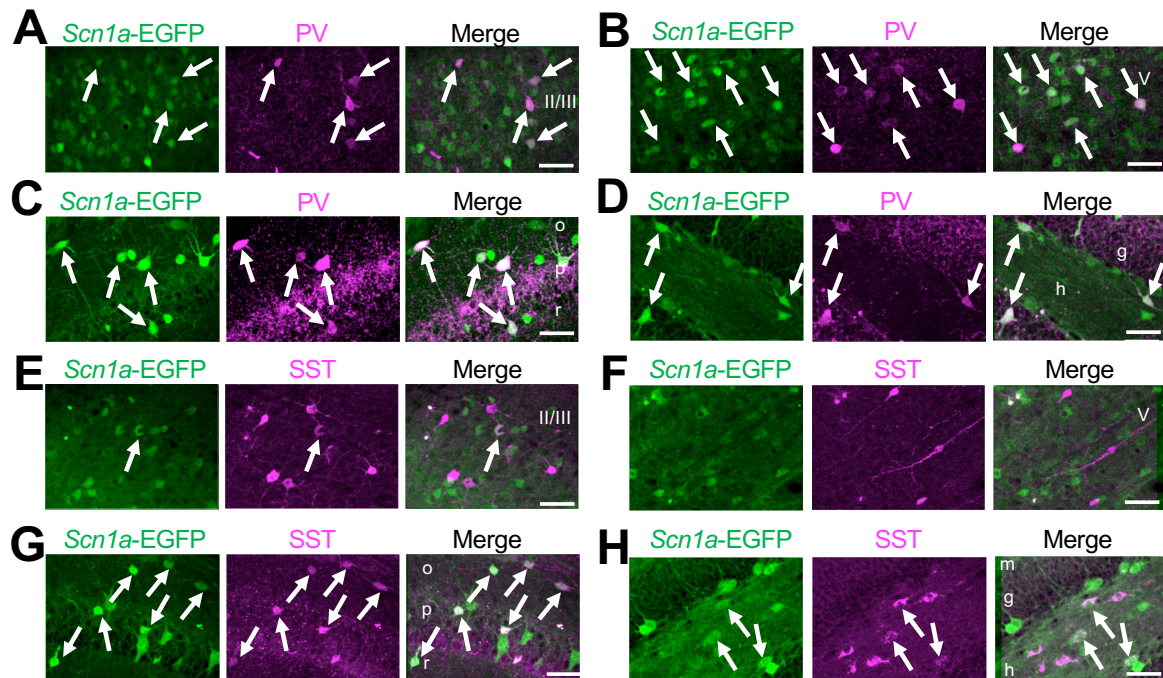
Supplemental figure S1. Cells with intense GFP (Nav1.1)-signals in *Scn1a*-GFP mouse neocortex and hippocampus are inhibitory neurons.

Immunofluorescence images of neocortical and hippocampal slices from 8-week-old *Scn1a*-GFP mice (line #233) indicate that intense GFP-signals (green) overlap with interneuron markers (magenta), parvalbumin (PV) **(A-D)** or somatostatin (SST) **(E-H)**. Merged images were shown in the right column. Arrows indicate the double-positive cells. o, stratum oriens; p, stratum pyramidale; r, stratum radiatum; h, hilus; g, stratum granulosum; m, stratum moleculare. All images are oriented from pial surface (top) to callosal (bottom). Scale bar; 50 μm.
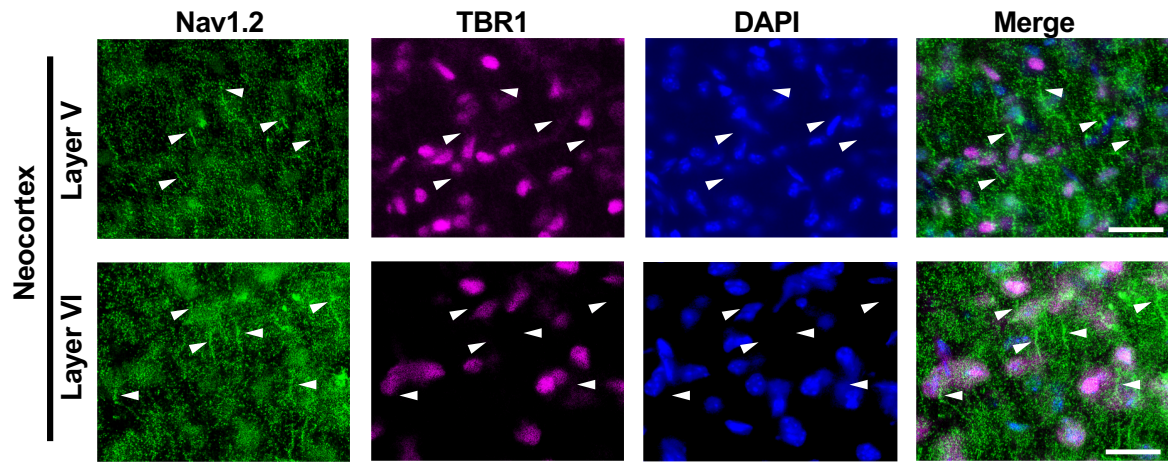
Supplemental figure S2. A major population of AISs of TBR1-positive cells are Nav1.2-positive at mouse neocortical layer V/VI

Immunofluorescence images of neocortical L5/6 of C57BL/6J at P15 stained with rabbit anti-Nav1.2 (green), alexa 647-conjugated anti-TBR1 (magenta) antibodies, and DAPI (blue). Arrowheads indicate TBR1-positive cells that have Nav1.2-positive AIS. Scale bars: Scale bars: 20μm.

Neuron markers		TBR1		FEZF2	
Region [a] **Age** [b]		**% GFP/TBR1** [c]	**% TBR1/GFP** [c]	**% GFP/FEZF2** [c]	**% FEZF2/GFP** [c]
L2/3	P15	71.9± 0.4	45.1± 0.7	43.2± 13.89	16.1± 4.9
	4w	64.7± 1.6	54.4± 0.7	48.2± 18.52	5.8± 0.3
L5	P15	7.3 ± 7.3	10.0 ± 3.5	83.4 ± 2.9	54.3 ± 2.2
	4w	5.1 ± 3.9	4.1 ± 3.2	95.7 ± 0.4	49.0 ± 1.2
	P15	15.4± 9.2	41.5± 12.9	8.0± 5.0	12.0± 9.6
L6	4w	25.6± 5.7	61.2± 2.9	36.2± 0.4	17.0± 3.7

Supplemental table S1. Ratios of GFP (Nav1.1)-positive, TBR1-positive or FEZF2-positive cells in *Scn1a*-GFP mouse (#233) neocortex.

L2/3, L5, L6: neocortical layer II/III, V, VI. P15: postnatal day 15, 4w: 4-week-old (N = 2, each age). Values are presented as mean ± SEM.